

Binary Black Hole Mergers within the LIGO Horizon: Statistical Properties and prospects for detecting Electromagnetic Counterparts

Rosalba Perna¹, Martyna Chruslinska², Alessandra Corsi³, Krzysztof Belczynski⁴

¹ *Department of Physics and Astronomy, Stony Brook University, Stony Brook, NY, USA*

² *Warsaw University Observatory, Al Ujazdowskie 4, 00-478 Warszawa, Poland*

³ *Department of Physics, Texas Tech University, Box 41051, Lubbock, TX 79409-1051, USA*

⁴ *Nicolaus Copernicus Astronomical Centre, Polish Academy of Sciences, ul. Bartycka 18, 00-716 Warsaw, Poland*

1 September 2017

ABSTRACT

Binary black holes (BHs) are one of the endpoints of isolated binary evolution, and their mergers a leading channel for gravitational wave events. Here, using the evolutionary code STARTRACK, we study the statistical properties of the BH-BH population from isolated binary evolution for a range of progenitor star metallicities and BH natal kicks. We compute the mass function and the distribution of the primary BH spin a as a result of mass accretion during the binary evolution, and find that this is not an efficient process to spin up BHs, producing an increase by at most $a \sim 0.2$ – 0.3 for very low natal BH spins. We further compute the distribution of merger sites within the host galaxy, after tracking the motion of the binaries in the potentials of a massive spiral, a massive elliptical, and a dwarf galaxy. We find that a fraction of 10-30% of mergers in massive galaxies and of 40-60% in dwarfs (range mostly sensitive to the natal kicks) is expected to occur outside of their hosts. Correspondingly, these mergers would be ‘naked’, and no significant afterglow radiation would be expected. We then consider the distribution of afterglow luminosities for the mergers occurring within the hosts and find that, if the energetics inferred for the candidate counterpart to GW 150914 detected by *Fermi* were typical, and the emission isotropic, a fraction of the order of ~ 40 – 70% (~ 20 – 50%) of the mergers in massive galaxies within the LIGO horizon could also be detectable in X-rays (radio).

Key words: gravitational waves — stars: black holes — gamma -ray burst: general

1 INTRODUCTION

The LIGO discovery of gravitational waves (GWs) from BH-BH mergers (Abbott et al. 2016c,a, 2017) has opened a new window onto the universe, providing a definite confirmation that binary BHs exist, and merge with a local rate in the range ~ 12 – $213 \text{ Gpc}^{-3} \text{ yr}^{-1}$ (Abbott et al. 2016e, 2017).

The properties of the LIGO-discovered BHs, and in particular the large masses and relatively low spins, have triggered numerous investigations aimed at identifying the possible formation channels of BHs with such properties. Three main mechanisms have been considered: Classical isolated binary evolution, dynamical formation, and chemically homogeneous evolution in tidally distorted binary stars. Within the classical isolated binary evolution scenario, the binary system undergoes a common envelope ejection, or a non-conservative mass transfer (e.g. Tutukov & Yungelson 1993; Kalogera et al. 2007). Dynamical formation involves

dynamical interactions in dense star clusters (e.g., Sigurdsson & Hernquist 1993; Antonini et al. 2016). For example, isolated BHs can acquire a companion via 3-body exchanges and binary-mediated interactions, which tend to result in the ejections of the lightest BH. Finally, for a chemically homogeneous evolution in tidally distorted binary stars, strong internal mixing occurs as a result of massive stars being in near contact binaries (e.g., de Mink et al. 2009).

During the first (O1) and second (O2) observing runs of advanced LIGO, a massive follow-up campaign in search for electromagnetic (EM) counterparts to GWs has been undertaken (e.g. Abbott et al. 2016b; Copperwheat et al. 2016; Cowperthwaite et al. 2016; Evans et al. 2016; Kasliwal et al. 2016; Morokuma et al. 2016; Palliyaguru et al. 2016; Savchenko et al. 2016; Smartt et al. 2016b,a; Bhalerao et al. 2017; Corsi et al. 2017; Kawai et al. 2017; Racusin et al. 2017; Savchenko et al. 2017). A combined GW-EM detection

has in fact enormous potential: it would help break GW parameter degeneracies, it would enable measurement of the source redshift, and help constrain the formation channel of the BH-BH binary by probing the environment in which the merger occurred.

To date, most searches for EM counterparts to the LIGO detections have yielded negative results. Possible exceptions are the potential γ -ray counterparts to GW 150914 and GW 170104 identified by the *Fermi* (Connaughton et al. 2016, but see Greiner et al. 2016) and AGILE (Verrecchia et al. 2017) satellites, respectively. While in NS-NS and NS-BH mergers EM emission is a natural outcome of the circularization, and subsequent accretion, of some mass from the tidally disrupted NS, in the case of BH-BH mergers no EM emission is generally expected. Thus, the tentative γ -ray detections by the *Fermi* and AGILE satellites have received considerable attention, and spurred several ideas to explain the possible origin of EM counterparts to BH-BH mergers in γ -rays (e.g. Perna, Lazzati & Giacomazzo 2016; Zhang 2016; Loeb 2016; Woosley 2016; Liebling & Palenzuela 2016), and at other wavelengths (i.e. Murase et al. 2016; de Mink & King 2017; Kimura, Murase & Mészáros 2017).

Given the large localization areas of GW events detected by LIGO (Abbott et al. 2016d), being able to design an EM follow-up strategy which optimizes the chances of detection is of paramount importance. The very first step toward this goal is gaining a better theoretical understanding of the relation between BH-BH binary properties, their merger sites, and the expected brightness of their potential EM counterparts. However, to date, there exists no specific prediction as to the most likely sites of BH-BH mergers within their host galaxies, and hence as to what afterglow brightness could be expected if these mergers were to give rise to explosive, gamma-ray burst (GRB)-like counterparts.

In light of the above, goal of this paper is to make statistical predictions for the observable properties of BH-BH mergers, and their possible EM counterparts, within the specific evolutionary model of isolated binary evolution, and within the standard GRB afterglow model (e.g., Sari, Piran & Narayan 1998) for the production of EM counterparts at various wavelengths. We build upon previous work of our group addressed at NS-NS and NS-BH mergers (Perna & Belczynski 2002; Belczynski et al. 2006). Using the code STARTRACK (Belczynski et al. 2008), we predict: (i) the BH-BH chirp and total mass distribution for several combinations of model assumptions and metallicities; (ii) the distribution of merger sites within their host galaxies; (iii) the increase in the spin distribution of the primary BH due to accretion from the secondary for several values of the initial spin; (iv) the expected afterglow luminosities in the X-ray, optical, and radio bands. For this last calculation, we take as a prototype the energetics inferred for the possible γ -ray counterpart to GW 150914 (Connaughton et al. 2016). While this detection may be spurious (Greiner et al. 2016), we use it here simply as a potential calibration point that may need to be changed when (and if) a secure BH-BH EM counterpart is detected. Hence, we present our results in a way such that they can be easily rescaled to different energy values.

The paper is organized as follows: the description of the galactic potentials used is detailed in Sec. 2, while Sec. 3 describes the population synthesis calculation, our model

assumptions, and the initial conditions for the simulations. Sec. 4 presents the computation of the afterglow spectrum under the assumption that merger events drive a shock in the interstellar medium. The results of our calculations are reported in Sec. 5, and include the distributions for the chirp and total mass function, the spin distribution of the primary BH, and the probability function for the location of merger events within their host galaxies, for several combinations of the metallicity and other relevant model parameters. The predicted electromagnetic luminosities are provided in three relevant bands. We summarize in Sec. 6.

2 GALAXY POTENTIAL MODELS

We consider three galaxy models: a large, Milky Way-type spiral galaxy, a large elliptical, and a dwarf galaxy. The latter is motivated by recent suggestions (O’Shaughnessy et al. 2017) that dwarf galaxies may overabundantly produce compact binary mergers, and particularly binary BHs. The type of galaxy is important for two reasons: (i) its potential determines the motion of the binaries, for given initial speeds and locations; (ii) its medium density (in magnitude and spatial distribution) influences the brightness of potential EM counterparts (afterglows). We follow the motion of the BH-BH binaries in the model galaxies from their formation time until the merger (for those which merge within a Hubble time), taking into account the kick velocities gained at the formation of each compact object.

The model spiral galaxy consists of a disc and a bulge described by the Miyamoto & Nagai (1975) type potential:

$$\Phi_{MN} = -\frac{GM}{\sqrt{x^2 + y^2 + (a + \sqrt{z^2 + b^2})^2}} \quad (1)$$

and a dark matter halo described by the Paczynski (1990) potential,

$$\Phi_{halo} = \begin{cases} -\frac{GM}{2R_{core}} \left[\log \left(1 + \frac{r^2}{R_{core}^2} \right) + \frac{R_{core}}{r} \operatorname{atg} \left(\frac{r}{R_{core}} \right) \right] & r < R_{cut} \\ -\frac{GM}{r} + \frac{GM}{R_{cut}} - \frac{GM}{2R_{core}} \left[\log \left(1 + \frac{R_{cut}^2}{R_{core}^2} \right) + \frac{R_{core}}{R_{cut}} \operatorname{atg} \left(\frac{R_{cut}}{R_{core}} \right) \right] & r > R_{cut}. \end{cases} \quad (2)$$

Our model elliptical galaxy consists of a bulge described by the (Hernquist 1990) type potential:

$$\Phi_H = -\frac{GM_E}{r + a_E} \quad (3)$$

and a halo with potential given by Eq. (2).

The parameters of the spiral galaxy potential are taken to be the same as those of the Milky Way: for the disc, $a = 4.2$ kpc, $b = 0.198$ kpc, $M = 8.78 \times 10^{10} M_{\odot}$; for the bulge, $a = 0$, $b = 0.277$ kpc, $M = 1.2 \times 10^{10} M_{\odot}$; and for the halo, $M_{halo} = 5 \times 10^{10} M_{\odot}$, $R_{core} = 6$ kpc, $R_{cut} = 100$ kpc. For the elliptical galaxy we assume a mass of $M_E = 5 \times 10^{11} M_{\odot}$ and a scale factor of $a_E = 5$ kpc, while the halo parameters are assumed to be the same as those for the spiral galaxy. The fraction of mass in gas is assumed to be $f_{gas} = 0.5$ for the bulge and disk, and $f_{gas} = \Omega_b/\Omega = 0.04$ for the halo (Bahcall et al. 1999).

For the case of the spiral galaxy, binaries are initially

placed on circular orbits in the disc. We adopt the distribution of stars within the disc of a spiral galaxy after Paczynski (1990):

$$P(R, z) dRdz = P(R)dR p(z)dz \quad (4)$$

where:

$$P(R)dR = a_R e^{-R/R_{exp}} \frac{R}{R_{exp}^2} dR \quad (5)$$

$$R = \sqrt{x^2 + y^2} \quad (6)$$

$$a_R = \left[1 - e^{-R_{max}/R_{exp}} \left(1 + \frac{R_{max}}{R_{exp}} \right) \right]^{-1} \quad (7)$$

and

$$p(z)dz = e^{-z/z_{exp}} \frac{1}{z_{exp}} dz, \quad (8)$$

with $R_{exp} = 4.5$ kpc, $R_{max} = 20$ kpc, and $z_{exp} = 75$ pc.

In the case of the elliptical galaxy, binaries are placed in the galactic bulge with random orientation of the orbital angular momentum, and with a mass density corresponding to the Hernquist potential, $\rho(r) = (M_E/2\pi)a_E r^{-1}(a_E + r)^{-3}$.

To model the dwarf galaxy, we take as a proxy a small spiral galaxy, of total mass (disk + halo + bulge) $M_{gal} = 1.5 \times 10^9 M_\odot$. Each individual mass component is rescaled to 0.1% of the corresponding one for the large spiral, while the spatial scale parameters of the potential are correspondingly rescaled to 10%.

3 BH-BH POPULATION SYNTHESIS MODELS

To obtain the population of double BH binaries, we use the STARTRACK population synthesis code, described in detail in Belczynski, Kalogera & Bulik (2002); Belczynski et al. (2008), with the updated treatment of the common envelope phase (as described in Dominik et al. 2012), and the wind mass loss (Belczynski et al. 2010).

3.1 Initial Conditions and Model Parameters

For binaries with periods < 3000 days, we adopt the initial conditions as described in Sana et al. (2012), based on spectroscopic observations of Galactic O-type stars: Kroupa-like IMF (IMF Kroupa, Tout & Gilmore 1993) with the power-law exponent modified to -2.3 for the stars of mass $M > 1.0 M_\odot$, eccentricity distribution $f(e) \propto e^{-0.42}$ in the range $[0.0, 1.0]$, period distribution $f(P) \propto [\log(P)/\text{days}]^{-0.55}$ in the range $[0.15, 3.48]$ and a flat binary mass ratio distribution $q = M_b/M_a$, within $[0.0, 1.0]$. Wider systems cannot be reliably probed through spectroscopic observations (Sana et al. 2012). Here, based on the recent review of Duchêne & Kraus (2013), for systems with initial periods of over 3000 days, we adopt a mass ratio distribution $f(q) \sim q^\gamma$ with $\gamma = -0.5$. There is no clear evidence for the period distribution to change considerably with periods increasing over 3000 days; we thus keep the rest of initial distributions of Sana et al. (2012) unchanged and extend the period distribution up to $\log[P/\text{days}] = 5.5$.

We study in depth three evolutionary models, chosen to give the largest spread in natal kicks, as detailed in Sec. 3.2. For clarity and consistency with other published works, we

keep the notation consistent with the one adopted by Belczynski et al. (2016a), and hence we use the same names for the models that we study. More specifically, we will consider models M10 (standard model), M13 and M15. These are the equivalent of models M1, M3 and M5 studied by Belczynski et al. (2016b), except that they include the effect of Pair-instability Pulsation Supernovae (PPSN) and Pair-instability Supernovae (PSN)¹.

The reference model (M10) has the minimum mass of the primary $M_{\text{mina}} = 20 M_\odot$, and minimum mass of the secondary $M_{\text{minb}} = 15 M_\odot$, while the maximum allowed mass for a main sequence star is $M_{\text{max}} = 150 M_\odot$. The other models (M13/M15) have a minimum mass of the primary equal to $M_{\text{mina}} = 5 M_\odot$, a minimum mass of the secondary given by $M_{\text{minb}} = 3 M_\odot$, and maximum allowed mass as in M10 ($M_{\text{max}} = 150 M_\odot$). For each model, we run three sets of metallicities: $Z_{\text{sun}} = 0.02, 10\% Z_{\text{sun}}, 1\% Z_{\text{sun}}$ (the contribution to the merging population is the biggest for small metallicities, see Belczynski et al. 2016c). Since the dependence of the remnant masses on metallicity is much stronger than the dependence on the of center-of-mass kicks, which (as we explain in what follows) vary among the models M10/M13/M15, we show results at different metallicities only for the M1 (standard) model. For this model, 2×10^7 isolated binaries from the above mass range were simulated for each metallicity, starting from zero-age main sequence (ZAMS) stars. For models M13 and M15, we simulated 2×10^7 and 2×10^6 binaries at ZAMS, respectively.

3.2 Natal kicks

Natal kicks play a fundamental role in determining the location of the merger sites within the host galaxies (and hence the medium density encountered by a potential GRB-driven shock). Models M10/M13/M15 make the following different assumptions for the natal kicks. In model M10, natal kicks gained by the newly formed BH during the supernova explosion are drawn from a Maxwellian distribution with the velocity dispersion $\sigma = 265 \text{ km s}^{-1}$, as proposed by Hobbs et al. (2005) based on observations of proper motions of single, young pulsars, but their values are lowered proportionally to the amount of material falling back onto the compact object (see Eq. 16 of Fryer et al. 2012). This model also accounts for a Blaauw kick velocity (a few km/s), gained by the center of mass of the binary due to mass loss during supernova explosion (Blaauw 1961). The amount of fallback matter increases with the BH mass, hence more massive BHs receive smaller natal kicks. Moreover, the most massive ones ($M_{\text{BH}} \gtrsim 10 M_\odot$ at solar metallicity) form through direct collapse, with no supernova explosion, and thus receive no birth kick. On the other hand, in the 'pessimistic' model M13, BHs receive full natal kicks drawn from a Maxwellian with $\sigma = 265 \text{ km s}^{-1}$ (which leads to birth velocities of the individual components of $\sim 400 \text{ km/s}$), but this time the kicks are not decreased due to fallback. Finally, model M15 has intermediate kicks drawn from a Maxwellian distribution with

¹ For the results presented here, the main difference between the models with and without PPSN/PSN is in the high mass BH range, $M_{\text{BH}} \gtrsim 40 M_\odot$, hence only of relevance for the tail of the mass function of the $Z = 1\% Z_\odot$ model.

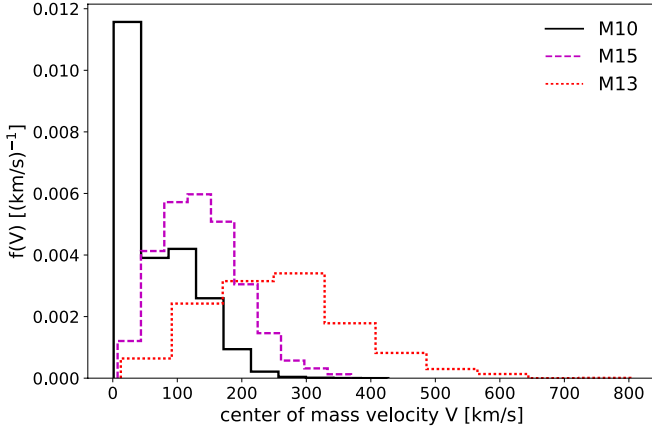


Figure 1. The BH-BH center of mass velocity distribution after the formation of the second BH, for the three models under consideration.

the lower velocity dispersion of $\sigma = 130 \text{ km s}^{-1}$ (equivalent of the M15 model in Belczynski et al. 2016b).

In order to get a better sense of the role of the natal kicks in the results for the merger locations within the host galaxies that will be shown in Sec.5.1, Fig. 1 shows the BH-BH center of mass velocity distribution after the formation of the second BH, for the three models under consideration and $Z = 10\%Z_{\odot}$ ² (but the metallicity has very little influence compared to the different model assumptions discussed above).

3.3 Binary Evolution

In the following, we provide a brief outline of our simulations and the main assumptions behind them. More details can be found in Belczynski et al. (2016b) and references therein.

- (i) Each binary system is followed from the ZAMS phase, and its evolution is assumed to proceed in isolation.
- (ii) Binary parameters (mass of the primary, mass ratio, eccentricity, separation/period) are randomly drawn from the distributions described in the previous section.
- (iii) The binary evolution includes simulations of tides, wind mass loss, and interaction between the components via mass transfer. These are modeled following the prescriptions detailed in Belczynski et al. (2008). Depending on the specific combination of parameters of each system, the binary may reach the point where the first compact object can form, or not (for instance, it can merge during the unstable mass transfer).
- (iv) If there is a supernova, a certain amount of mass is lost instantaneously; the magnitude of the natal kick velocity is drawn from the assumed distribution (as described in the previous section), with a random direction. The magnitude of the natal kick, the amount of ejecta, and the parameters of the binary at the moment of the explosion determine whether the binary will be disrupted or not.

² We adopt $Z_{\odot} = 0.02$ (Villante et al. 2014).

(v) The evolution of the binary is followed until the formation of the second compact object, or until the merger/disruption of the binary (if this happens before the formation of the double compact object system).

(vi) Given the final orbital parameters and the masses of each binary, we can then calculate the merger time due to gravitational radiation. Here we follow only the binaries which merge within the Hubble time.

3.4 BH Spin Evolution due to accretion

Our formalism for the computation of the change in BH spin as a result of BH accretion follows the literature (Shakura & Sunyaev 1973; Thorne 1974). In particular, we adopt the formalism of Brown et al. (2000), also used by Belczynski et al. (2008).

The spin parameter of a BH of mass M_{BH} and angular momentum J is defined as

$$a = \frac{Jc}{M_{\text{BH}}^2 G}, \quad (9)$$

where G is the gravitational constant and c the speed of light. If a BH with angular momentum J_i accretes an amount of material with rest mass M_{acc} , its new angular momentum will be given by

$$J = J_i + J_{\text{acc}}, \quad (10)$$

where

$$J_{\text{acc}} = \left[\frac{R_{\text{iso}}^2 - \tilde{a}\sqrt{2R_{\text{Sch}}R_{\text{iso}}} + \tilde{a}^2}{R_{\text{iso}}(R_{\text{iso}}^2 - \frac{3}{2}R_{\text{Sch}}R_{\text{iso}} + \tilde{a}\sqrt{2R_{\text{Sch}}R_{\text{iso}}})^{1/2}} \right] \times cM_{\text{acc}}\sqrt{\frac{R_{\text{Sch}}R_{\text{iso}}}{2}}. \quad (11)$$

Here $R_{\text{Sch}} = 2GM_{\text{BH}}/c^2$ is the BH Schwarzschild radius, $\tilde{a} \equiv J_i/M_{\text{BH}}c = a_i(GM_{\text{BH}}/c^2)$, with a_i the initial BH spin; R_{iso} is the radius of the last stable orbit

$$R_{\text{iso}} = \frac{R_{\text{Sch}}}{2} \{3 + r_2 - [(3 - r_1)(3 + r_1 + 2r_2)]^{1/2}\} \quad (12)$$

with

$$r_1 = 1 + \left(1 - \frac{4\tilde{a}^2}{R_{\text{Sch}}^2}\right)^{1/3} \left[\left(1 + \frac{2\tilde{a}}{R_{\text{Sch}}}\right)^{1/3} + \left(1 - \frac{2\tilde{a}}{R_{\text{Sch}}}\right)^{1/3} \right]$$

and

$$r_2 = \left(3\frac{4\tilde{a}^2}{R_{\text{Sch}}^2} + r_1^2\right)^{1/2}. \quad (13)$$

Note that, as the BH accretes mass, its gravitational mass increases as

$$M_{\text{BH},f} = M_{\text{BH}} + \frac{E}{c^2}, \quad (14)$$

where

$$E = M_{\text{acc}}c^2 \left[\frac{R_{\text{iso}}^2 - R_{\text{Sch}}R_{\text{iso}} + \tilde{a}\sqrt{R_{\text{Sch}}R_{\text{iso}}/2}}{R_{\text{iso}}(R_{\text{iso}}^2 - \frac{3}{2}R_{\text{Sch}}R_{\text{iso}} + \tilde{a}\sqrt{2R_{\text{Sch}}R_{\text{iso}}})^{1/2}} \right]. \quad (15)$$

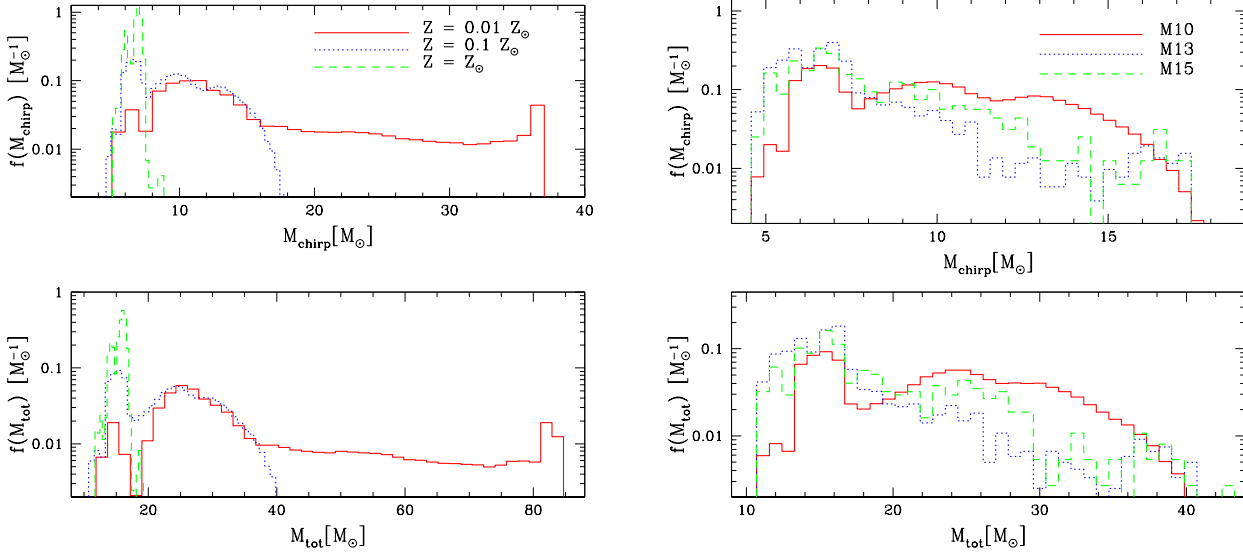


Figure 2. *Left:* The distribution of chirp masses (*top panel*) and of total masses (*bottom panel*) for the BH remnants (in the source frame) for three values of the metallicity, in the M10 model. *Right:* Same distributions as in the left panel, but for the 3 models studied here, at 10% of solar metallicity. Note that the dependence of the remnant mass fraction on metallicity is much stronger than variations in the mass function produced by different model assumptions for the natal kicks.

4 AFTERGLOW MODEL FOR EM COUNTERPARTS

As discussed in Sec. 1, whether BH-BH mergers can be accompanied by a release of energy in the form of a relativistic outflow, is a completely open question at the moment. With these uncertainties and caveats in mind, in the following we will make the basic assumption that, if the merger of two BHs is accompanied by a sudden energy release, it will lead to a relativistic shockwave propagating into the medium. Radiation is expected as a result of synchrotron emission by shock-accelerated electrons. We compute such emission within the standard synchrotron model developed by Sari, Piran & Narayan (1998) for a relativistic, adiabatic shock. The electrons are assumed to have a power-law distribution of Lorentz factors γ above a minimum value γ_m , and are able to lose rapidly energy to radiation if their γ is larger than a threshold value γ_c . The resulting spectral energy distribution is then (e.g., Sari, Piran & Narayan 1998)

$$F_\nu = F_{\nu, \max} \begin{cases} (\nu/\nu_c)^{1/3}, & \nu < \nu_c \\ (\nu/\nu_c)^{-1/2}, & \nu_c \leq \nu < \nu_m \\ (\nu_m/\nu_c)^{-1/2}(\nu/\nu_m)^{-p/2}, & \nu \geq \nu_m \end{cases}, \quad (16)$$

where $\nu_c \equiv \nu(\gamma_c)$ and $\nu_m \equiv \nu(\gamma_m)$.

On the other hand, if the criterium $\gamma_c > \gamma_m$ is satisfied, only electrons with $\gamma_e > \gamma_c$ can cool efficiently. Under this condition, the spectrum takes the functional form (e.g., Sari,

Piran & Narayan 1998)

$$F_\nu = F_{\nu, \max} \begin{cases} (\nu/\nu_m)^{1/3}, & \nu < \nu_m \\ (\nu/\nu_m)^{-(p-1)/2}, & \nu_m \leq \nu < \nu_c \\ (\nu_c/\nu_m)^{-(p-1)/2}(\nu/\nu_c)^{-p/2}, & \nu \geq \nu_c \end{cases}. \quad (17)$$

In the above equations, the parameter p represents the power-law index of the electron energy distribution. The maximum flux intensity is achieved when $F_\nu = F_{\nu, \max}$, where (Sari, Piran & Narayan 1998)

$$F_{\nu, \max} = 110 n^{1/2} \xi_B^{1/2} E_{52} d_{28}^{-2} (1+z) \text{ mJy}. \quad (18)$$

This formalism assumes that the magnetic field energy density in the shock rest frame is a fraction ξ_B of the equipartition value, and the electrons carry a fraction ξ_e of the dissipated energy. E_{52} is the explosion energy in units of 10^{52} erg, while d_{28} is the luminosity distance in units of 10^{28} cm, and t_d is the time in days, as measured in the observer frame, since the beginning of the burst. The relevant frequencies at which the spectral index changes are the cooling frequency ν_c (corresponding to energies at which radiative losses over the shock's lifetime are significant) and the synchrotron frequency ν_m (the minimal energy of the radiating electrons), respectively given by the following expressions (Sari, Piran & Narayan 1998)

$$\nu_c(t) = 2.7 \times 10^{12} n_1^{-1} \xi_B^{-3/2} E_{52}^{-1/2} t_d^{-1/2} (1+z)^{-1/2} \text{ Hz}, \quad (19)$$

and (Sari, Piran & Narayan 1998)

$$\nu_m(t) = 5.7 \times 10^{14} \xi_e^2 \xi_B^{-1/2} E_{52}^{1/2} t_d^{-3/2} (1+z)^{1/2} \text{ Hz}. \quad (20)$$

Additionally, at low frequencies, synchrotron self-absorption can become important. The self-absorption frequency below

which the spectrum becomes optically thick is given by (Yost et al. 2003)

$$\nu_a(t) = 4.2 \times 10^8 f(p) (\xi_e^*)^{-1} \xi_B^{0.2} E_{52}^{0.2} n^{0.6} (1+z)^{-1} \text{ Hz}, \quad (21)$$

where $f(p) = [(p+2)(p-1)/(3p+2)]^{0.6}$ and $\xi_e^* = \xi_e(p-2)/(p-1)$. Below this frequency, the spectrum declines more rapidly, as ν^2 .

5 RESULTS

5.1 Chirp mass, total mass, and merger sites

The left panel of Fig. 2 shows the distribution of chirp mass, $M_{\text{chirp}} = M_1^{3/5} M_2^{3/5} (M_1 + M_2)^{-1/5}$, and of total mass, $M_{\text{tot}} = M_1 + M_2$, for our three representative metallicities in model M10, while the right panel shows the same distributions for $Z = 10\% Z_\odot$, and our three representative models (M10/M13/M15). Note that, for relatively low mass GW events, the GW signal in the LIGO sensitive frequency band is dominated by the inspiral phase, and the chirp mass is the most accurately measured parameter. As expected, the mass distribution has a strong metallicity dependence, reflecting the significant amount of mass lost to winds during the evolution of the more metal rich progenitor stars. On the other hand, the dependence on the specific model at the same metallicity is considerably weaker, with model M10 displaying an enhancement in mass at the higher end of the distribution. This results from the larger amount of fallback for the more massive BHs.

In Fig. 3 we show the distribution of projected distances (from the galaxy center) of the merger sites for our three representative models and the three galaxy types. Since the distributions are dependent only very weakly on the progenitor stars metallicity, we show just the case of $Z = 0.1 Z_\odot$. The orientation angle of the galaxy with respect to the line of sight in each Monte Carlo realization is drawn from a random distribution. All three models predict a sizable fraction of mergers to occur at very large distances, with a fraction $\sim 10 - 30\%$ (depending on the model) expected to occur outside of spiral and elliptical galaxies (formal size set at 100 kpc). As expected, model M13, with the largest natal kicks for the BHs, is the one which predicts the largest fraction of mergers to be located at the largest distances. The fraction of BH-BH merger events expected to occur outside of dwarf hosts (formal size set at 10 kpc) is larger, ranging from $\sim 40\%$ in the model with the smallest natal kicks to $\sim 60\%$ in the model with the largest kicks. This larger fraction is expected as a result of the shallower potential of the dwarf galaxy.

As a reference for the observability of a putative EM counterpart, the figure also shows, with vertical lines, the projected distances corresponding to 1 arcsec for a galaxy at the three representative redshifts of $z = 0.05, 0.1, 0.2$, all within the aLIGO horizon, at least for the most massive BHs. This shows that observational facilities with sub-arcsec localization capabilities could measure potential counterpart off-sets / positions within the host galaxy.

For the computation of afterglow-like EM radiation accompanying BH-BH mergers, the ambient density of the medium at the merger sites plays an important role, since the afterglow peak flux scales as $n^{1/2}$ (see Eq. 18). Fig.

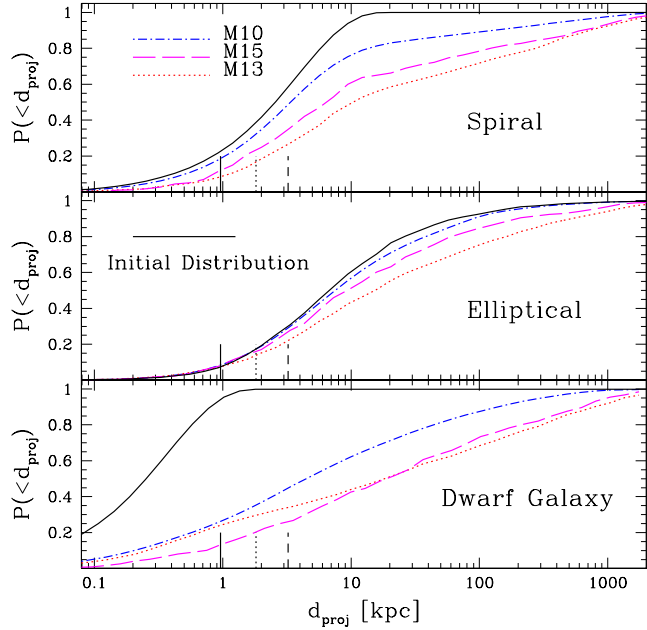


Figure 3. The fraction of BH-BH binaries which merge within a projected distance d_{proj} of their host galaxy center. Distances are the largest in the M13 model, reflecting the larger kicks at birth. A fraction $\sim 10 - 30\%$ (with precise value dependent on the model) is expected to be found outside of their elliptical / spiral hosts (formal size set to 100 kpc). The fraction of BH-BH merger events expected to occur outside of dwarf hosts (formal size set to 10 kpc) is larger ($\sim 40 - 60\%$) due to the shallower galaxy potential. For each model, the dependence of distances on metallicity is negligible, hence only the $Z = 0.1 Z_\odot$ case is shown. The three vertical lines correspond to an angular distance of 1 arcsec for a galaxy at a redshift of $z = 0.05$ (solid line), $z = 0.1$ (dotted line) and $z = 0.2$ (dashed line).

4 shows the number density distribution predicted by our models, for evolution in a spiral, elliptical, and dwarf galaxy. Higher ambient densities are generally expected in model M10, given the smaller distances that the binaries have traveled prior to merging. Correspondingly, this scenario will predict brighter afterglows, as quantified in Sec. 5.3.

5.2 Spin evolution of the primary BH as a result of accretion during binary evolution

In the binary evolutionary scenario under consideration, the calculation of the spins that we perform – following the formalism described in Sec. 3.4 – and report on here refers to the evolution of the spin of the primary BH (i.e. the BH born first, which is typically the more massive of the two BHs at merger time) as a result of mass accretion from the companion star during evolution. As evident by Eq. (10), the angular momentum (and hence the spin) of the BH follow-

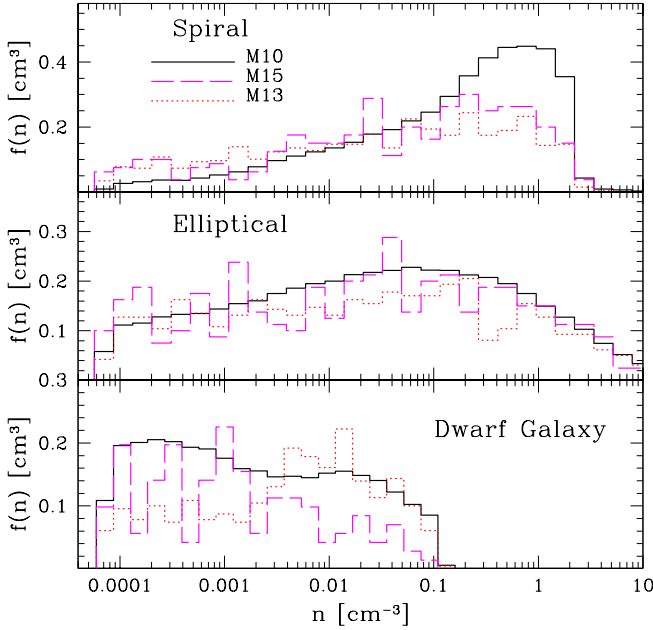


Figure 4. The density distribution at the sites of BH-BH mergers, for our galaxy potentials and three evolutionary models. Densities tend to be higher in the M10 model, reflecting the smaller natal kicks of the BHs. The densities around the merger sites are important for the possible production of a shock-driven afterglow.

ing accretion depends on the amount of angular momentum possessed by the accreted mass, as well as on the initial angular momentum possessed by the BH immediately following the supernova (SN) explosion. Since the distribution of BH spins following the SN explosion is not well known, here we perform calculations for three initial values of the primary BH spin (namely $a_{\text{in}} = 0, 0.25, 0.5$), so that the net effect of the increase due to accretion (which we accurately compute here) can be immediately inferred.

The left panel of Fig. 5 shows the expected spin distribution in model M10 for the three representative metallicities and an initial BH spin equal to zero. In all the cases, the spin gained by the BHs is rather marginal. The distribution peaks at $a \sim 0.1$, for the 1% and 10% solar metallicities, and at $a \sim 0.2$ for the solar metallicity case. The larger spin acquired by the BHs from higher metallicity stars is due to the fact that, while the accreted mass during the common evolution phase is not significantly dependent on metallicity, however, the mass of the BHs which are accreting is typically smaller at higher metallicities, hence resulting in a larger spin.

The middle panel of Fig. 5 shows the final spin distribution for model M10 at 10% metallicity, for three initial values of the initial spin of the BHs at birth. The general trend is that of a relatively smaller increase for the largest initial

spins, as expected. Last, the right panel shows the dependence of the spin distribution on the different evolutionary model assumptions. Compared to model M10, models M13 and M15 display a longer tail of larger spins. This is mainly due to the fact that model M10 produces a relatively higher fraction of more massive BHs compared to models M13 and M15.

So far, LIGO measurements of BH spin magnitudes have been inconclusive. This originates from the fact that gravitational waveforms are not very sensitive to BH spins, unless the BH spins are high and precess around (are tilted with respect to) the binary angular momentum. In the four current BH-BH merger detections (GW150914, LVT151012, GW151226, GW170104) no significant precession was measured, and only in one event (GW151226) a non-zero spin magnitude of at least one BH is required.

Our results show that accretion in progenitor binaries of massive BH-BH mergers is not an efficient process to spin up BHs. For very low natal BH spins ($a_{\text{in}} \approx 0$), the final BH spin is not larger than 0.2–0.3, and for higher initial BH spins ($a_{\text{in}} \gtrsim 0.5$) the BH spin remains almost unaffected by accretion. This is a direct result of the fact the accretion onto a BH in the common envelope phase (the major accretion event for typical BH-BH progenitor) is not estimated to occur at rates much higher than a few percent of the Bondi rate (Ricker & Taam 2008; MacLeod & Ramirez-Ruiz 2015; Murguia-Berthier et al. 2017). In other words, our results show that LIGO will be measuring the natal BH spin in BH-BH mergers if they originate from the classical formation scenario discussed here (Belczynski et al. 2016b). This is of fundamental importance, since BH natal spins can be potentially used to infer information about the angular momentum/rotation of the massive stars progenitors of these BHs. Rotation and angular momentum transport in massive stars are basic missing blocks of stellar evolution theory.

If, for example, LIGO BHs are found to typically have very low spins, it will indicate that angular momentum is lost rather effectively from massive stars, and the Tayler-Spruit dynamo (Spruit 1999) may be a process that operates in massive stars. However, that would also indicate that LIGO BHs originate from a different population than Galactic and extra-galactic High-Mass X-ray Binaries, which all show very high spins ($a \gtrsim 0.9$; see Tab.1 in Fragos & McClintock 2015). If, on the other hand, BH spins were to be found to be generally high, it would mean that angular momentum transport is a rather inefficient process (i.e. the core must decouple from the envelope early on in the massive star evolution). In this last case, a variety of long GRB central engines based on single massive star progenitors (e.g., MacFadyen & Woosley 1999), could also be realized in BH-BH mergers. Last, if a mixed population (low and high spins) of LIGO BHs is found by future detections, it will point to mild coupling of layers within a massive rotating star, moderated by the effects of wind mass loss that depends on star mass and metallicity (e.g., Geneva stellar models; Eggenberger, Montalbán & Miglio 2012; Georgy et al. 2013). Such a model would naturally explain high spins of low mass BHs (like the ones observed in HMXB in very local Universe), along with low spin BHs that have high masses ($M_{\text{BH}} \gtrsim 20 - 30 M_{\odot}$; Belczynski et al. 2017).

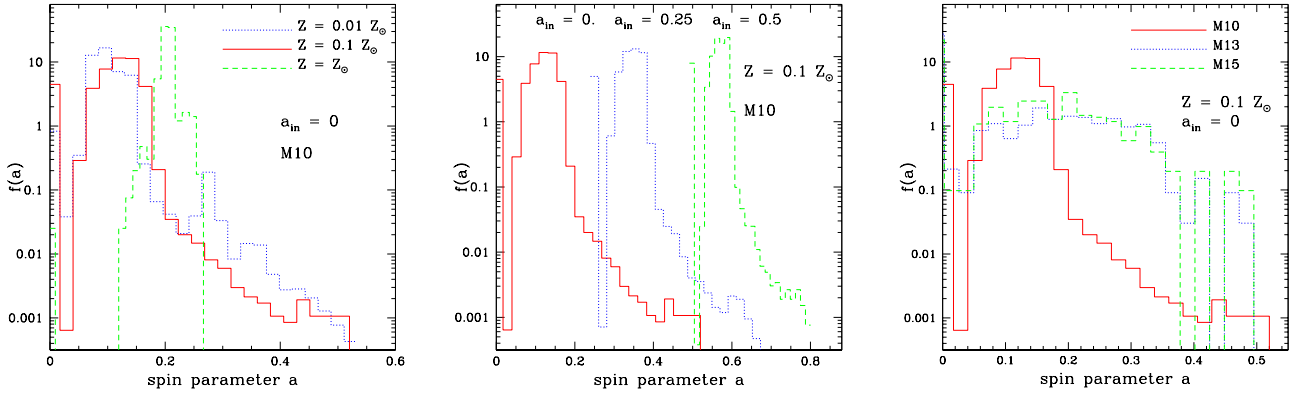


Figure 5. The distribution of the spin parameter of the primary BH due to accretion of matter from the companion during the binary evolution. *Left:* Dependence on metallicity for the M10 model, assuming that the initial spin of the BH (following the SN explosion) is zero. *Middle:* Dependence of the spin distribution on the initial BH spin, for the M10 model at 10% of solar metallicity. *Right:* The spin distribution in the three evolutionary models studied here, at 10% metallicity and assuming zero initial spin.

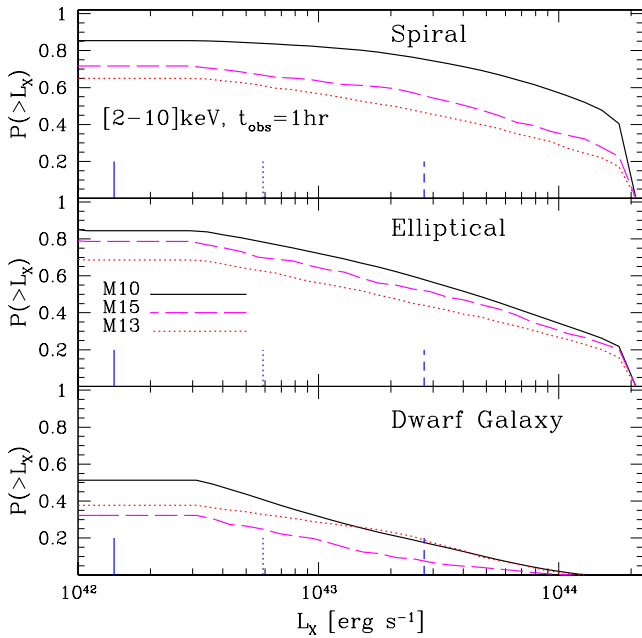


Figure 6. The cumulative probability distribution of afterglow luminosities in the 2–10 keV band at 1 hr after the burst. The vertical lines indicate the minimum luminosity that would be detectable by *Swift*/XRT (unabsorbed 2–10 keV flux of $F_{\text{lim}} \approx 2.5 \times 10^{-13} \text{ erg s}^{-2} \text{ cm}^{-2}$, see text) for a burst located at $z = 0.05$ (solid line), $z = 0.1$ (dotted line), $z = 0.2$ (dashed line), respectively. Note that the probabilities do not saturate at 1, reflecting the fraction of much dimmer afterglows resulting from mergers outside of the host galaxy, in the intergalactic medium.

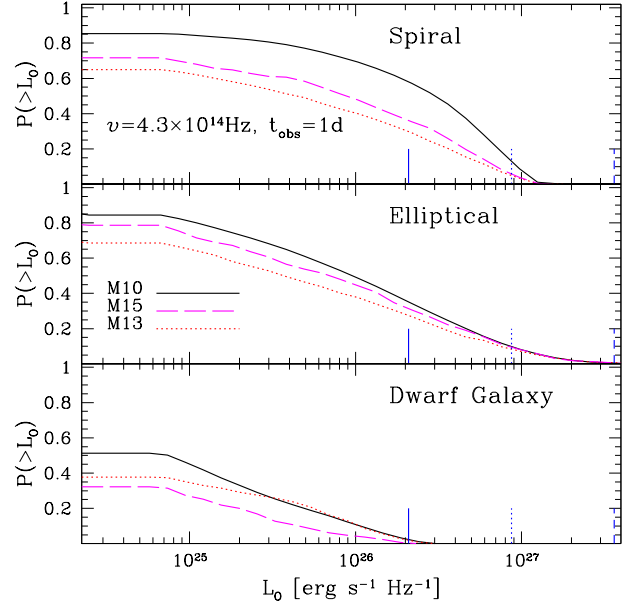


Figure 7. Same as in Fig.6, but at the frequency of $\nu = 4.3 \times 10^{14} \text{ Hz}$ (falling in the R band) at 1 day after the burst. A limiting flux of $F_{\text{lim}} \approx 4 \mu\text{Jy}$ (see text) has been assumed to set the values of the minimum luminosity for detection at a redshift of 0.05 (solid line), 0.1 (dotted line), 0.2 (dashed line).

5.3 EM counterparts to BH-BH mergers

In the following, we use the radiation model described in Sec.4, coupled with the density distribution at the BH-BH merger sites calculated in Sec. 5.1, to estimate the expected brightness distribution of afterglows possibly associated with BH-BH merger events.

We compute the predicted afterglow luminosities under

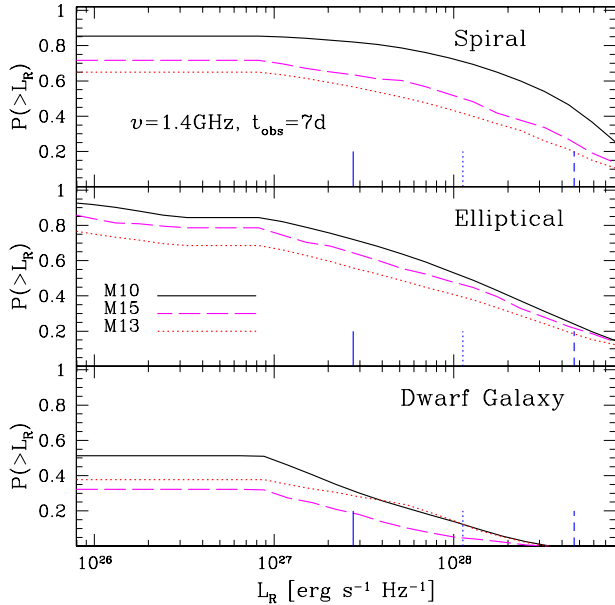


Figure 8. Same as in Figs. 6 and 7 but in the radio (1.4 GHz) at 7 days after the burst. A limiting flux of $F_{\text{lim}} = 50 \mu\text{Jy}$ (see text) has been assumed to set the values of the minimum luminosity for detection at a redshift of 0.05 (solid line), 0.1 (dotted line), 0.2 (dashed line).

the assumption that each BH-BH merger event is associated with an explosive release of energy. As discussed in Sec. 1, we take as a representative case the energetics of the candidate γ -ray counterpart to GW 150914 reported by the *Fermi* collaboration (Connaughton et al. 2016), i.e. $E = 10^{49}$ erg. We then adopt $\xi_B = 0.01$ and $\xi_e = 0.1$, as typical values inferred from broad-band afterglow modeling in the ‘standard’ GRBs (Wijers & Galama 1999; Panaitescu & Kumar 2001). Adopting a single value for E, ξ_B, ξ_e (rather than assuming some arbitrary distributions) allows us to (a) highlight the dependence on the different evolutionary models (which predict different merger sites and hence medium densities), and (b) present results that can be immediately rescaled to other values of these parameters (which may be motivated by future observations), thanks to the analytical dependence of the afterglow flux on these parameters (see Sec.4).

Fig. 6 shows the distribution of afterglow luminosities in the 2-10 keV band at 1 hr after the merger for our three representative models and three galaxy types. Since, as discussed above, the merger sites have very little dependence on metallicity, we only show results for $Z = 10\%Z_\odot$. The vertical lines indicate the minimum luminosity that would be detectable by *Swift*/XRT in a follow-up search with sensitivity similar to the one achieved for GW 150914 ($F_{\text{lim}} \approx 2.5 \times 10^{-13}$ erg s $^{-2}$ cm $^{-2}$ in the 2-10 keV band; see Abbott et al. 2016b) for a burst located at the three representative redshifts of $z = 0.05, 0.1, 0.2$ (all within the LIGO BH-BH horizon). The probability of detecting an X-ray counterpart is in the range of 65-85% depending on the evolutionary model and galaxy type for the closest el-

liptical/spiral galaxy, and between 40-70% for the farthest galaxy. A larger fraction of brighter events is expected in the M10 model, due to the generally smaller distances (and hence higher densities) of the merger sites from the galaxy centers. Note that the probabilities flatten out at low luminosities with values < 1 as a result of fact that a fraction of BH-BH mergers is predicted to occur outside of the host galaxy, in the intergalactic medium. The luminosities of those events (which would bring the total cumulative probabilities to 1) are lower than the lowest limit in the figure. In the case of dwarf hosts, for the same emission parameters (E, ξ_e, ξ_B) used for the massive galaxies, the luminosities are lower, due to the smaller number densities. Additionally, a larger fraction of events is expected to be ‘naked’, due to the mergers occurring outside the host. This fraction can be directly read from the flattening of the probability distributions at low luminosities: up to a fraction ~ 30 -50% (depending on the magnitude of the natal kicks and the redshift of the host) could have a non-negligible afterglow-like EM counterpart.

Fig. 7 shows the same distributions, but in the optical after 1 day. The vertical lines, corresponding to the minimum detectable luminosity for events at the same representative redshifts as in Fig. 6, have been computed assuming a 5σ limiting magnitude of $r \approx 22.4$ mag (AB system, equivalent to a limiting flux of $F_{\text{lim}} \approx 4 \mu\text{Jy}$), comparable to the most sensitive optical searches carried out in this band during the follow-up of GW 150914 (see Table 1 in Abbott et al. 2016b). An inspection of Fig. 7 shows that detection in the optical is not likely for a merger in a dwarf galaxy, even at a low redshift of $z \sim 0.05$. For massive galaxies, the detection probability becomes more sizeable, but only at low redshifts. In particular, for $z = 0.05$, a fraction between 30-60% of events could be detected in the optical. This fraction becomes 10% or smaller already at $z = 0.1$.

Fig. 8 shows the probability distributions in the radio band, at 1.4 GHz after 1 week from the explosive event. Here, the reference threshold flux corresponding to the minimum detectable luminosities at the redshifts of 0.05, 0.1, 0.2 is set at the 5σ threshold flux for the Karl G. Jansky VLA (A configuration) for 1 hr integration on-source ($F_{\text{lim}} \approx 50 \mu\text{Jy}$). For mergers at a redshift of 0.2, corresponding to the highest redshift LIGO BH-BH merger so far (Abbott et al. 2017), about 25-45% of events could be detected as radio afterglows, depending on the model and galaxy type, for massive galaxies, while for dwarf galaxies the detection probability is non-negligible only at lower redshifts, being about 20% for events at $z = 0.1$. Note that, for the particular choice of afterglow parameters adopted here (namely E, ξ_e, ξ_B), and the range of densities probed by the merger events, the afterglow spectrum is in the regime described by the middle branch of Eq. (18). In this case, the flux at the same observation time is higher at lower frequencies. However, given the sensitive parameter dependences of Eq. (19) and Eq. (20), the frequency-dependence across the bands can be reversed for other combinations of the relevant parameters.

We finally note that, up to this point, our calculations have estimated the brightness of possible afterglow counterparts independently of their visibility due to beaming effects. However, an afterglow-like EM counterpart to a GW event may come from a relativistic jet of size $\theta_{\text{jet}} < \pi/2$. Under these circumstances, our computed probabilities for the ob-

servability of afterglow-like emission should be reduced by the beaming factor $(1 - \cos\theta_{\text{jet}})$ if interpreted as detection probability of an EM counterpart following a GW event independently of a γ -ray detection. As an example, for a double jet with semi-conical size $\theta_{\text{jet}} \sim 10^\circ$, the beaming factor is ~ 0.015 .

6 SUMMARY

In light of the detection of GWs from BH-BH mergers, and the massive efforts at searching for EM counterparts from such events, here we have performed a study aimed at predicting the statistical properties of the merged BH-BH population within their host galaxies, for BHs produced via massive stars evolution in isolated binaries. In addition to calculating the mass function (provided in terms of both chirp and total mass), for three values of the metallicity, we have computed the spin distribution of the primary BH as a result of accretion of mass from the secondary during the close binary evolution. Of particular importance for optimizing follow-up strategies, we provided the expected distance distribution within the galaxy potential, for a massive spiral, a massive elliptical, and a dwarf galaxy (modeled as a scaled-down version of a spiral). We considered the two most extreme models (as well as one in between) for the kicks received by the BHs at birth. As such, our results span the expected range for BH-BH mergers within the isolated binary scenario. The distribution of the merger sites directly translates (for a given galaxy model) into a distribution for the number density of the interstellar medium, and hence into afterglow luminosities, for given choices of the burst parameters. Our results can be summarized as follows:

(i) The mass function has a strong metallicity dependence, as expected. A chirp mass $\sim 20 M_\odot$ requires metallicities $\lesssim 0.1 Z_\odot$. The influence of natal kicks is much weaker than the influence of metallicity on the BH-BH merger mass function.

(ii) The accreted mass from the progenitor star of the secondary BH to the primary BH during the period of mass transfer increases the BH spin by an amount which, in the standard model M10 is about 0.1 for 0.01% and 0.1% Z_\odot , and about 0.2 for Z_\odot . The increase, for the same amount of accreted mass, is slightly smaller for larger initial natal spins of the primary BH. For the same initial conditions, models M13 and M15 produce a generally larger fraction of high spin BHs, with a flat spin distribution up to $a \sim 0.35$ if the initial spin of the primary BH is zero.

(iii) The distribution of merger sites (and hence of projected distances/angular offsets) within the host galaxies spans a large range of values, with a fraction $\sim 10 - 30\%$ for massive galaxies (with precise value depending on the model and galaxy type) occurring outside of the galaxy, at distances $R \gtrsim 100$ kpc. This fraction of mergers outside of the hosts is larger ($\sim 40 - 60\%$) for a dwarf galaxy, here modeled as a spiral with mass of 0.1% that of the Milky Way. As expected, in the model with the largest natal kicks (M13), there is a larger fraction of mergers occurring outside of the galaxy, and more generally at larger distances from the center. These offsets could be easily measured by any observational facility with sub-arcsec localization capabilities, if the merger is associated with EM emission.

(iv) Using the distribution of interstellar medium densities derived from the distribution of merger sites within the host galaxies, and assuming that BH-BH events produce GRB-like counterparts similar to the *Fermi* candidate counterpart to GW 150914, we have computed the resulting afterglow distributions in the X-rays, optical, and radio band. We find that, for massive galaxies, a fraction on the order of $10 - 30\%$ of the mergers (where the precise value depends on the assumed natal kick distribution and galaxy type) is expected to be naked, i.e. lacking a bright afterglow at any wavelength. The same fraction is higher, $\sim 40 - 60\%$, in dwarf galaxies. These events correspond to mergers that occur outside of the host galaxy, within the diffuse intergalactic medium.

A fraction of the order of $\sim 40 - 70\%$ (depending on the model and galaxy type) of the mergers in massive galaxies would be accompanied by broad-band afterglow-like emission detectable in X-rays if occurring within the LIGO horizon and if associated with a γ -ray signal similar to the *Fermi* candidate counterpart to GW 150914. A smaller fraction could also be detectable at radio and optical wavelengths with sensitive enough follow-up instruments. Given the analytical scaling of afterglow flux with energy, our results can be easily scaled should future observations indicate positive detection but point to different values of the energetics.

Acknowledgments. RP was partly supported for this work by NSF award AST-1616157. KB acknowledges support from the Polish National Science Center (NCN) grant: Sonata Bis 2 (DEC-2012/07/E/ST9/01360). AC acknowledges support from the NSF CAREER award #1455090.

REFERENCES

- Abbott B. P. et al., 2016a, *Physical Review Letters*, 116, 241103
 —, 2016b, *ApJ*, 826, L13
 —, 2016c, *Physical Review Letters*, 116, 061102
 —, 2016d, *Living Reviews in Relativity*, 19, 1
 —, 2016e, *ApJ*, 833, L1
 —, 2017, *Phys. Rev. Lett.*, 118, 221101
 Antonini F., Chatterjee S., Rodriguez C. L., Morscher M., Pattabiraman B., Kalogera V., Rasio F. A., 2016, *ApJ*, 816, 65
 Bahcall N. A., Ostriker J. P., Perlmutter S., Steinhardt P. J., 1999, *Science*, 284, 1481
 Belczynski K., Bulik T., Fryer C. L., Ruiter A., Valsecchi F., Vink J. S., Hurley J. R., 2010, *ApJ*, 714, 1217
 Belczynski K. et al., 2016a, *A&A*, 594, A97
 Belczynski K., Holz D. E., Bulik T., O’Shaughnessy R., 2016b, *Nature*, 534, 512
 Belczynski K., Kalogera V., Bulik T., 2002, *ApJ*, 572, 407
 Belczynski K., Kalogera V., Rasio F. A., Taam R. E., Zezas A., Bulik T., Maccarone T. J., Ivanova N., 2008, *ApJS*, 174, 223
 Belczynski K. et al., 2017, *ArXiv e-prints*
 Belczynski K., Perna R., Bulik T., Kalogera V., Ivanova N., Lamb D. Q., 2006, *ApJ*, 648, 1110
 Belczynski K., Repetto S., Holz D. E., O’Shaughnessy R., Bulik T., Berti E., Fryer C., Dominik M., 2016c, *ApJ*, 819, 108
 Bhalerao V. et al., 2017, *ArXiv e-prints*

- Blaauw A., 1961, *Bull. of the Astr. Inst. of the Netherlands*, 15, 265
- Brown G. E., Lee C.-H., Wijers R. A. M. J., Bethe H. A., 2000, *Physics Reports*, 333, 471
- Connaughton V. et al., 2016, *ApJ*, 826, L6
- Copperwheat C. M. et al., 2016, *MNRAS*, 462, 3528
- Corsi A. et al., 2017, *ArXiv e-prints*
- Cowperthwaite P. S. et al., 2016, *ApJ*, 826, L29
- de Mink S. E., Cantiello M., Langer N., Pols O. R., Brott I., Yoon S.-C., 2009, *A&A*, 497, 243
- de Mink S. E., King A., 2017, *ApJ*, 839, L7
- Dominik M., Belczynski K., Fryer C., Holz D. E., Berti E., Bulik T., Mandel I., O’Shaughnessy R., 2012, *ApJ*, 759, 52
- Duchêne G., Kraus A., 2013, *ARAA*, 51, 269
- Eggenberger P., Montalbán J., Miglio A., 2012, *A&A*, 544, L4
- Evans P. A. et al., 2016, *MNRAS*, 462, 1591
- Fragos T., McClintock J. E., 2015, *ApJ*, 800, 17
- Fryer C. L., Belczynski K., Wiktorowicz G., Dominik M., Kalogera V., Holz D. E., 2012, *ApJ*, 749, 91
- Georgy C., Ekström S., Granada A., Meynet G., Mowlavi N., Eggenberger P., Maeder A., 2013, *A&A*, 553, A24
- Greiner J., Burgess J. M., Savchenko V., Yu H.-F., 2016, *ApJ*, 827, L38
- Hernquist L., 1990, *ApJ*, 356, 359
- Hobbs G., Lorimer D. R., Lyne A. G., Kramer M., 2005, *MNRAS*, 360, 974
- Kalogera V., Belczynski K., Kim C., O’Shaughnessy R., Willems B., 2007, *Physics Reports*, 442, 75
- Kasliwal M. M. et al., 2016, *ApJ*, 824, L24
- Kawai N., Negoro H., Serino M., Mihara T., Tanaka K., Masumitsu T., Nakahira S., 2017, *ArXiv e-prints*
- Kimura S. S., Murase K., Mészáros P., 2017, *ArXiv e-prints*
- Kroupa P., Tout C. A., Gilmore G., 1993, *MNRAS*, 262, 545
- Liebling S. L., Palenzuela C., 2016, *PRD*, 94, 064046
- Loeb A., 2016, *ApJ*, 819, L21
- MacFadyen A. I., Woosley S. E., 1999, *ApJ*, 524, 262
- MacLeod M., Ramirez-Ruiz E., 2015, *ApJ*, 798, L19
- Miyamoto M., Nagai R., 1975, *PASJ*, 27, 533
- Morokuma T. et al., 2016, *PASJ*, 68, L9
- Murase K., Kashiyama K., Mészáros P., Shoemaker I., Senno N., 2016, *ApJ*, 822, L9
- Murguia-Berthier A. et al., 2017, *ApJ*, 835, L34
- O’Shaughnessy R., Bellovary J. M., Brooks A., Shen S., Governato F., Christensen C. R., 2017, *MNRAS*, 464, 2831
- Paczynski B., 1990, *ApJ*, 348, 485
- Palliyaguru N. T. et al., 2016, *ApJ*, 829, L28
- Panaiteescu A., Kumar P., 2001, *ApJ*, 560, L49
- Perna R., Belczynski K., 2002, *ApJ*, 570, 252
- Perna R., Lazzati D., Giacomazzo B., 2016, *ApJ*, 821, L18
- Racusin J. L. et al., 2017, *ApJ*, 835, 82
- Ricker P. M., Taam R. E., 2008, *ApJ*, 672, L41
- Sana H. et al., 2012, *Science*, 337, 444
- Sari R., Piran T., Narayan R., 1998, *ApJ*, 497, L17
- Savchenko V. et al., 2017, *ArXiv e-prints*
- , 2016, *ApJ*, 820, L36
- Shakura N. I., Sunyaev R. A., 1973, *A&A*, 24, 337
- Sigurdsson S., Hernquist L., 1993, *Nature*, 364, 423
- Smartt S. J. et al., 2016a, *MNRAS*, 462, 4094
- , 2016b, *ApJ*, 827, L40
- Spruit H. C., 1999, *A&A*, 349, 189
- Thorne K. S., 1974, *ApJ*, 191, 507
- Tutukov A. V., Yungelson L. R., 1993, *MNRAS*, 260, 675
- Verrecchia F. et al., 2017, *ArXiv e-prints*
- Villante F. L., Serenelli A. M., Delahaye F., Pinsonneault M. H., 2014, *ApJ*, 787, 13
- Wijers R. A. M. J., Galama T. J., 1999, *ApJ*, 523, 177
- Woosley S. E., 2016, *ApJ*, 824, L10
- Yost S. A., Harrison F. A., Sari R., Frail D. A., 2003, *ApJ*, 597, 459
- Zhang B., 2016, *ApJ*, 827, L31